RSC Advances

RSC Advances

www.rsc.org/advances

This is an *Accepted Manuscript*, which has been through the Royal Society of Chemistry peer review process and has been accepted for publication.

Accepted Manuscripts are published online shortly after acceptance, before technical editing, formatting and proof reading. Using this free service, authors can make their results available to the community, in citable form, before we publish the edited article. This *Accepted Manuscript* will be replaced by the edited, formatted and paginated article as soon as this is available.

You can find more information about *Accepted Manuscripts* in the **Information for Authors**.

Please note that technical editing may introduce minor changes to the text and/or graphics, which may alter content. The journal's standard **Terms & Conditions** and the **Ethical guidelines** still apply. In no event shall the Royal Society of Chemistry be held responsible for any errors or omissions in this *Accepted Manuscript* or any consequences arising from the use of any information it contains.

ROYAL SOCIETY OF CHEMISTRY

www.rsc.org/advances

Journal Name

ARTICLE TYPE

Hybrid Ni-Al layered double hydroxide/graphene composite supported gold nanoparticles for aerobic selective oxidation of benzyl alcohol

M. Y. Miao, J. T. Feng *, Q. Jin, Y. F. He, Y. N. Liu, Y. Y. Du, N. Zhang, D. Q. Li *

In this work, a Ni-Al layered double hydroxide/graphene (NiAl-LDH/RGO) nanocomposite which was synthesized by introducing NiAl-LDH on the surface of graphene oxide (GO) and simultaneously reducing graphene oxide without any additional reducing agents was utilized as the support for Au nanoparticles. Raman spectroscopy and XPS analysis revealed that NiAl-LDH/RGO composite had both
10 defect sites and oxygenic functional groups in RGO to control the directional growth of Au nanoparticles and lead to a small particle size. Compared to Au catalyst supported on single GO and RGO or NiAl-LDH, this composite-supported Au catalyst (Au/NiAl-LDH/RGO) exhibited superior catalytic activity and stability in the selective oxidation of benzyl alcohol using molecular oxygen under low pressure. Improved activity was mainly ascribed to the small Au particle size effect caused by RGO and the
15 contribution of basic sites in NiAl-LDH. Moreover, preferable catalytic stability of Au/NiAl-LDH/RGO catalyst was attributed to the defect sites and oxygenic functional groups in RGO which anchored the Au NPs and prevented the agglomeration, meanwhile, the agglomeration of RGO was inhibited by the introduction of NiAl-LDH.

INTRODUCTION

20 Selective oxidation of benzyl alcohol is an important reaction for the production of benzaldehydes, which are widely used both as high value components of dyestuffs, pharmaceuticals, perfumes, agrochemicals and as fine chemical intermediates.[1-4] The traditional process to produce benzaldehyde has many problems
25 such as the difficulty of product separation and the discharge of caustic liquid or gas. Direct oxidation of benzyl alcohol with molecular oxygen (O_2) as the terminal oxidant has attracted considerable attention from the viewpoint of green sustainable chemistry.[5] To date, developing catalysts for solvent-free
30 oxidation of benzyl alcohol with high activity and selectivity is still a fundamental challenge.[6] Compared with other noble metals (Pd, Pt, etc.), supported Au nanoparticles (NPs) with higher selectivity towards target product and stability, have been used as a promising catalyst in selective oxidation of benzyl alcohol.[7-9]
35 However, a common feature of Au NPs catalysts is the need of strongly alkaline medium (typically NaOH or K_2CO_3) which was believed to facilitate the β-hydride elimination step, making purification a challenge and limiting their industrial application.[10-12] An efficient way to circumvent these difficulties
40 is to develop new types of Au NPs supports that can be finely tuned with controllable surface properties to maximize the catalytic activity.[13]

Graphene, a unique crystal of monolayer carbon atoms, densely packed into a two-dimensional (2D) honeycomb
45 lattice,[14-17] has received tremendous attentions as a promising catalyst support due to its large specific surface area, outstanding corrosion resistance and excellent thermal conductivity.

Graphene oxide (GO) is the derivative of graphene,[18] it not only retains the advantages of graphene but also have certain amounts
50 of oxygenic functional groups such as hydroxyl, epoxide and carboxyl groups to promote the oxidation reaction.[19,20] By the process of chemical reduction, most of the oxygenic functional groups in GO could be reduced and leave behind lots of topological defects and carbon vacancies, while accomplishing
55 the transformation from GO to the reduced graphene oxide (RGO).[21] Because of the functional groups as well as the carbon vacancies and defects present in RGO, the sorption and intercalation of ions and molecules are possible.[22] This feature, together with the high specific surface area offers RGO a
60 promising candidate for catalyst supports in selective oxidation reaction. However, a major practical shortcoming of GO or RGO is the tendency to aggregate,[23,24] resulting in the decrease of catalytic activity and poor stability. To overcome such issues, it is considerable to bring in other guest functional materials to
65 modify them.[25]

Layered double hydroxides (LDHs), with the general formula of $[M_{1-x}^{2+}M_x^{3+}(OH)_2]^{x+}(A^{n-})_{x/n}\cdot mH_2O$, have attracted a great deal of interests in the application of heterogeneous catalysis because of their wide variety of properties such as the different metal
70 cations on hydrotalcite layer with tunable compositions, alkali property and thermal stability.[26-29] Taking advantages of the unique tunable properties, LDHs are suitable for fabricating graphene-based composites.[30,31] Li et al. reported the synthesis and catalytic performance of ZnCr-LDH/graphene composite as
75 the catalyst for visible-light-responsive photocatalytic toward rhodamine degradation.[32] They found that the growth of LDH on

the graphene sheets was very effective in preventing graphene sheets restack to form layered graphite structure. Furthermore, the alkali medium used for the growth of LDH could also simultaneously reduce GO to reduced graphene oxide (RGO), which has less oxygenic functional groups to improve the hydrophilicity of GO.[33] They also reported a graphene-supported Ni nanocatalyst prepared via self-reduction of hybrid Ni-Al layered double hydroxide/graphene and it exhibited superior catalytic performance in the liquid phase selective hydrogenation of cinnamaldehyde to hydrocinnamaldehyde.[34] To the best of our knowledge, utilizing LDH/graphene composites as the catalyst support for selective oxidation reaction has not been reported yet. Herein, in this work, we reported the research on the specific combination of NiAl-LDH and RGO as the support of Au catalyst for selective oxidation of benzyl alcohol. Initially, we synthesized GO by a modified Hummers method, whereafter, NiAl-LDH was prepared by coprecipitation method on the surface of GO, which involved the nucleation and growth of NiAl-LDH and the reduction of graphene oxide without the addition of any reducing agents. Au nanoparticles were then immobilized on the support of NiAl-LDH/RGO by using sol-immobilization method (Fig. 1). As comparison, Au nanoparticles were also loaded on pure GO, RGO and NiAl-LDH using the same method. XRD, FT-IR, TEM, Raman spectra, BET, ICP and XPS were employed to investigate the composition and structure of the catalysts and revealed the promotion effect of NiAl-LDH/RGO support on the catalytic performance for Au catalyst.
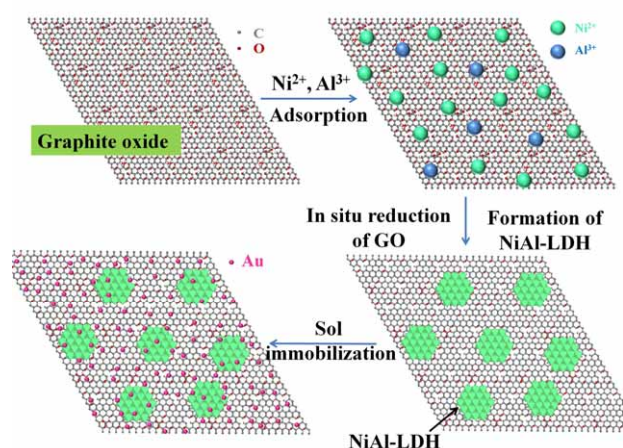

Fig.1 Schematic illustration of preparing the Au/NiAl-LDH/RGO catalyst.

Experimental Section

Materials

Purified natural graphite powder was purchased from Beijing OuHe Technologies co., ltd. Other reagents were A.R. grade and used without further purification. The water used in all the experiments was deionized and had an electrical conductivity less than 10^{-6} S·cm^{-1}.

Synthesis of NiAl-LDH/RGO composites

The starting material, graphite oxide (GO), was synthesized by a modified Hummers method. GO was exfoliated using an ultrasonication method in ultrasonic bath. NiAl-LDH/RGO composite was then fabricated directly by the coprecipitation method. A certain amount of GO was dispersed into 50 mL of a mixture of NaOH (14.0 mmol) and Na_2CO_3 (4.2 mmol) solution upon 30 min of ultrasonication. Next, both the mixture and another salt solution containing $Ni(NO_3)_2 \cdot 6H_2O$ (4.8 mmol) and $Al(NO_3)_3 \cdot 9H_2O$ (1.6 mmol) were added drop-wise together under vigorous stirring at room temperature to obtain a suspension. Subsequently, NaOH solution (0.2 M) was titrated with the solution for adjusting the pH value of the solution to 10.5. The suspension was then crystallized for the LDH phase for 10 h at 150 °C, followed by filtering and washing with deionized water until pH 7. The solid was dried at 60 °C for 12 h in a vacuum oven to obtain NiAl-LDH/RGO composite. For comparison, both the pure NiAl-LDH and RGO were prepared. The NiAl-LDH was fabricated in the absence of GO under the above identical experimental conditions, and the RGO was prepared by reducing GO in NaOH (0.8 M) solution.

Au/NiAl-LDH/RGO catalyst prepared by sol-immobilization method

Supported Au catalyst was prepared using a sol-immobilization method. An aqueous solution of $HAuCl_4 \cdot 3H_2O$ of the desired concentration, Poly(vinyl alcohol) (PVA) (1 wt% aqueous solution) and an aqueous solution of $NaBH_4$ (0.1 M) was prepared. The catalyst comprising Au nanoparticles with 1 wt% total metal loading on NiAl-LDH/RGO support was prepared as follows: The required amount of a PVA solution was added (PVA/Au (wt/wt)=1.2) to an aqueous $HAuCl_4$ solution; a freshly prepared solution of $NaBH_4$ ($NaBH_4$/Au (mol/mol)=5) was then added to form a dark-brown sol. After 2 h of sol generation, the colloid was immobilized by adding NiAl-LDH/RGO under vigorous stirring conditions at room temperature. After 2 h the slurry was filtered, the catalyst washed thoroughly with distilled water and dried at 60 °C overnight. This sample is denoted as Au/NiAl-LDH/RGO. For comparative study, Au catalysts supported on pure GO and NiAl-LDH were also prepared as stated above keeping the total metal loading of 1% wt and denoted as Au/GO, Au/RGO and Au/NiAl-LDH, respectively.

Characterizations

Powder XRD patterns were recorded on a Shimadzu XRD-600 X-ray powder diffractometer (Cu K$_\alpha$ radiation, λ = 0.15406 nm) between 3° and 70° 2θ, with a scan speed of 10° min^{-1}. Fourier transform infrared (FT-IR) spectra were recorded on a Bruker Vector 22 spectrometer using the KBr pellet technique (1 mg of sample in 100 mg of KBr). Transmission electron microscopy (TEM) was carried out on a Hitachi H-800 transmission electron microscope with an accelerating voltage of 100 kV. The Raman spectra were obtained on a Jobin Yvon Horiba HR800 spectrometer using a 532 nm line of Ar$^+$ ion laser as the excitation source at room temperature. BET surface area of catalyst supports was analyzed by low temperature N$_2$ adsorption/desorption method on a Micromeritics Surface Area & Porosity Gemini VII 2390 (before the BET measurement, the samples were degassed at 100 °C for 15 h). Elemental analysis was performed using a Shimadzu ICPS-75000 inductively coupled plasma emission spectrometer (ICP-ES) and an Elementar Vario EL elemental analyzer. X-ray photoelectron spectroscopy (XPS) was recorded on a VG ESCALAB 2201 XL spectrometer with a monochromatic Mg K$_\alpha$ X-ray radiation

(1253.6 eV photons). Binding energies were calibrated based on the graphite C 1s peak at 284.5 eV. The morphology and size distribution of the samples were examined using JEOL J-2100 high resolution transmission electron microscopy (HRTEM).

Benzyl alcohol oxidation

Benzyl alcohol oxidation was carried out in a stainless steal autoclave with a nominal volume of 100 ml. In a typical reaction, 400 mg catalyst and 40 mL benzyl alcohol were added into the reactor, and then purged with O_2 five times before closing and the pressure was maintained at 2 bar (relative pressure). The reactor with the reaction mixture was kept in a heating block, heating to 140 ^{o}C under vigorous stirring using a magnetic bar inside the reactor (stirring rate 1000 rpm). After 10 h reaction time, the reaction mixture was cooled down to room temperature and the catalyst was separated from the reaction mixture by centrifugation, thoroughly washed with acetone for recycle. During the reaction, an aliquot of the clear supernatant (0.5 mL) was periodically taken from the reaction mixture, filtered and diluted with mesitylene (0.5 mL, internal standard for GC analysis), and then analyzed by an Agilent 7890B gas chromatograph equipped with a flame ionisation detector and a 30 m CP-Wax 52 CB column. The products were identified by comparison with known standards. For the quantification of the amounts of reactants consumed and products generated, an internal standard method was used. The carbon mass balance was proved for the experiments with a maximal difference of ±5%.

Results and discussion

Characterization of NiAl-LDH/RGO composite
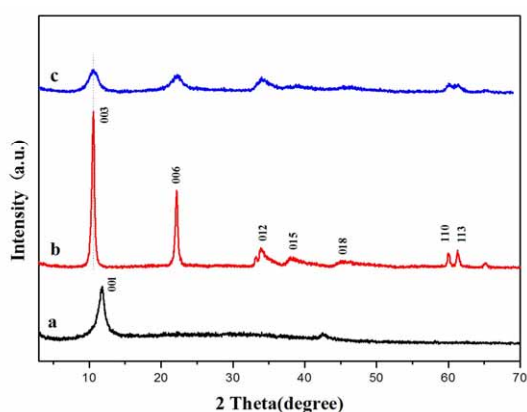
Fig. 2 XRD patterns of GO (a), NiAl-LDH (b) and NiAl-LDH/RGO (c).

Fig. 2 shows the powder XRD patterns of GO, NiAl-LDH and NiAl-LDH/RGO. The XRD pattern of the precursor GO shows a strong characteristic (001) diffraction at 2θ=11.5° (Fig. 2a), corresponding to an interlayer distance of 0.78 nm, which can be attributed to the formation of oxygenic functional groups on the graphite sheets[35] The pattern of NiAl-LDH (Fig. 2b) exhibits the two-dimensional hydrotalcite-like characteristic reflections of (003), (006), and (110) peaks, the d spacing value of the (003) diffraction peak of LDH phase is about 0.76 nm, demonstrating the intercalation of CO_3^{2-} anions into the interlayer of LDH.[36] As expected, no characteristic diffraction of GO was observed in the composite sample (Fig. 2c), which could be attributed to the

reduction of GO to RGO. However, the pattern of composite shows similar diffraction peaks with NiAl-LDH, suggesting the formation of NiAl-LDH, and the deposition of NiAl-LDH nanoplatelets on the surface of the resulting RGO weakened the surface energy of graphene sheets and inhibited the restacking of the exfoliated RGO.[37] Moreover, comparing NiAl-LDH/RGO composite to pure NiAl-LDH, there is an obvious decrease in the intensity of the diffraction peaks, due to the disorder in the stacked structure.[38]
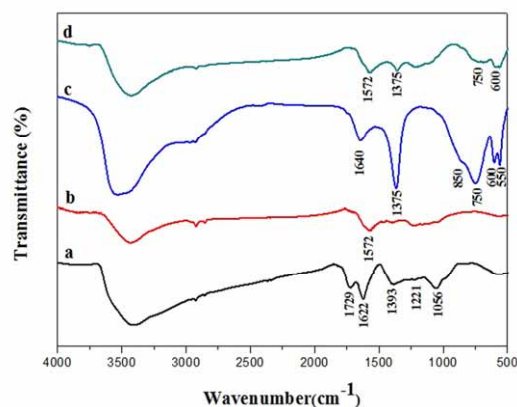
Fig. 3 FT-IR spectra of GO (a), RGO (b), NiAl-LDH (c) and NiAl-LDH/RGO (d).

The FT-IR spectra of GO, RGO, NiAl-LDH and NiAl-LDH/RGO samples are shown in Fig. 3. In the IR spectrum of GO (Fig. 3a), the absorption peak around 1729 cm^{-1} is assigned to C=O stretching vibration of −COOH groups, and the absorption around 1622 cm^{-1} is associated with the stretching vibration of carbon backbone (C=C/C−C).[35] The three stretching vibrations of C−OH, C−O−C and C−O are located around 1393, 1221, 1056 cm^{-1} respectively. In addition, the broad absorption bands between 3670 and 3260 cm^{-1} belonged to hydroxyl stretching band (ν O−H) caused by −COOH groups and water molecules.[39] For RGO obtained from the reduction of GO in NaOH solution (Fig. 3b), the most obvious broad absorption is at 1572 cm^{-1}, assigned to the skeletal aromatic vibration, other absorption peaks cannot be clearly identified. The FT-IR spectra of NiAl-LDH shown the peak of asymmetric stretching vibrations of carbonate anions at 1375cm^{-1}, [40] and the bands appearing at 600 cm^{-1} and 550 cm^{-1} are attributed to the characteristic bending vibrations of metal−oxygen (M−O) bond and metal−hydroxyl (M−OH) bond in the lattice of LDH.[41] However, as for NiAl-LDH/RGO, the absorption bands related to C=O and C−O stretching vibrations cannot be clearly observed comparing with pure GO. Meanwhile, the absorption peaks for the stretching vibrations of the carbon backbone (1572 cm^{-1}) and CO_3^{2-} anions (1375 cm^{-1}) were observed. The results of FT-IR spectra further confirmed the reduction of GO and the presence of LDH phases in the NiAl-LDH/RGO composite.
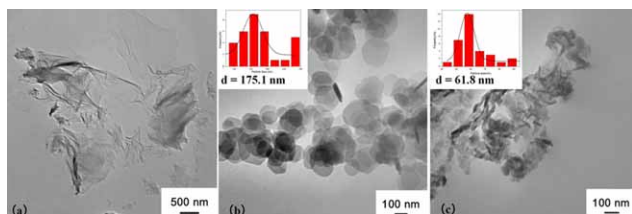
Fig. 4 TEM images of GO (a), NiAl-LDH (b), NiAl-LDH/RGO (c) and the size distribution of NiAl-LDH nanoplatelets.

The morphology and structure of GO, NiAl-LDH and NiAl-LDH/RGO were investigated by means of TEM measurements, as shown in Fig. 4 As for GO (Fig. 4a), a transparent ultrathin sheet structure with a few thin ripples within the flat surface can be observed, which shows that GO sheets were efficiently exfoliated.[31] The TEM image of NiAl-LDH/RGO (Fig. 4c) shows a marked contrast with pure GO, the thin graphene sheets were decorated densely by nanosized NiAl-LDH particles and no obvious aggregate is observed, which is in accord with the XRD patterns. The NiAl-LDH nanoplatelets grew parallel or perpendicular to the surface of RGO. It is worth mentioning that the average crystallite size of the NiAl-LDH in NiAl-LDH/RGO composites is about 61.8 nm, significantly lower than that of pure NiAl-LDH (Fig. 4b) obtained under the similar conditions (175.1 nm). Herein, we supposed that the oxygenic functional groups on the surface of GO could promote the sorption and intercalation of metal ions and act as anchoring sites for metal nanoparticles, which controlled the directional growth of NiAl-LDH nanoplatelets and led to a smaller particle size, consistent with other literature reports. [42, 43]
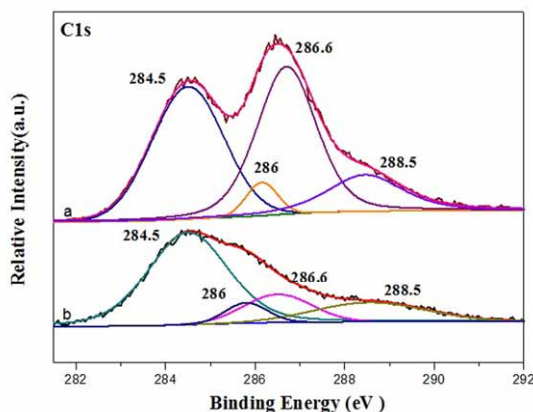

Fig. 5 C1s XPS of GO (a) and NiAl-LDH/RGO (b).

The chemical structure of GO and NiAl-LDH/RGO was further explored by the XPS technique. As shown in Fig. 5, the C1s spectra of both GO and NiAl-LDH/RGO can be deconvoluted into four separate peaks corresponding to different carbon bonds including $C=C$ and/or $C-C$ groups (284.5 eV), $C-OH$ groups (286.0 eV), $C-O-C$ groups (286.6 eV) and $-COOH$ groups (288.5 eV).[23] In the spectrum of GO (Fig. 5a), the peak area ratio of the oxygen-containing bonds to the total carbon bonds was calculated to be 60.07%, accounting for a large degree of oxidation. The plenty of oxygenic functional groups on the surface of GO could control the directional growth of NiAl-LDH nanoplatelets or Au NPs and therefore lead to a small particle size. However, some literatures reported that the superabundant

oxygenic functional groups in carbon materials could also result in over-oxidation of alcohols. [44] In contrast to pure GO, the peak areas of $C-OH$, $C-O-C$ and $-COOH$ groups for NiAl-LDH/RGO composite decreased significantly and the peak area ratio of the oxygen-containing bonds to the total carbon bonds reduced to 36.72%, which further proved the effective and sufficient reduction of GO to RGO during the in situ growth process of the NiAl-LDH. In this process, NaOH severing as the precipitating agent for NiAl-LDH formation could also provide alkaline ambient for the deoxygenation of oxygenic functional groups in GO.[32]
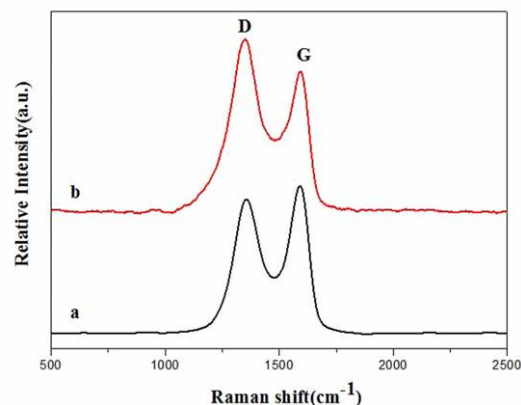

Fig. 6 Raman spectra of GO (a) and NiAl-LDH/RGO (b).

In the Raman spectra of GO and NiAl-LDH/RGO composites, the two intense peaks at around 1358 and 1590 cm^{-1} can be respectively assigned to the D band and G band of the carbon materials, which corresponding to the vibrations of carbon atoms with dangling bonds in plane terminations of disordered graphite and the first order scattering of sp^2 bonds of carbon atoms.[45] By quantitatively measuring the intensity ratio of the D and G bands (I_D/I_G), the ordered and disordered crystal structures of carbon can be evaluated. For the D/G band intensity ratio of NiAl-LDH/RGO composite ($I_D/I_G = 1.13$), there is an increased I_D/I_G intensity ratio in comparison with that of GO ($I_D/I_G = 0.90$), indicating that the composite decorated with NiAl-LDH nanoplatelets could lead to a more disordered structure. This result could be ascribed to the decrease in the size of the in-plane sp^2 domains as well as the increase of some un-repaired topological defects and carbon vacancies caused by the removal of oxygen functional groups from GO during the growth of NiAl-LDH nanoplatelets.[46] Similar to the oxygenic functional groups, the added defect sites on the surface of RGO in NiAl-LDH/RGO composite could also adsorb the metal ions and be utilized as anchoring centers for the nucleation and dispersion of the loading metal nanoparticles and lead to a smaller particle size.[47] In summary, even with less oxygenic functional groups, the NiAl-LDH/RGO composite could still impact the particle size distribution and surface morphology of the loaded Au NPs, as it has plenty of both defect sites and oxygenic functional groups.

Support effect and catalytic performance of the NiAl-LDH/RGO supported Au catalyst

In order to take into consideration the texture properties of Au/GO, Au/RGO, Au/NiAl-LDH and Au/NiAl-LDH/RGO, the Brunauer-Emmett-Teller surface areas (S_{BET}) of the different

supports were presented in Table 1, as well as the Au loading of the catalysts determined by ICP analysis. The S_{BET} of GO, RGO and NiAl-LDH were 136.93 m^2/g, 141.89 m^2/g and 61.18 m^2/g, respectively, and increased to 172.47 m^2/g after hybrid. In general, high surface area could lead to small particle size, high dispersion of active components, and therefore superior catalytic performance.[22] As for the experimental Au loadings employed in the final catalysts, the Au content in Au/GO is much lower than it in Au/NiAl-LDH with the same preparation process. Excluding the experimental errors, this phenomenon might be attributed to high hydrophilicity of GO leading to the loss in the preparation of catalyst. However, the Au loadings in Au/RGO and Au/NiAl-LDH/RGO is up to 0.65 wt. % and 0.66 wt. %, indicating that the RGO and NiAl-LDH/RGO composite have less oxygenic functional groups and therefore reduce the hydrophilicity of GO.
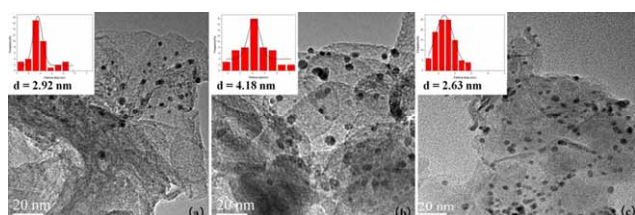

Fig. 7 HRTEM images and the size distribution of 1% Au/GO (a), 1% Au/NiAl-LDH (b), 1% Au/NiAl-LDH/RGO (c).

Fig. 7 shows the HRTEM images of the Au catalysts supported on GO, NiAl-LDH and NiAl-LDH/RGO and the corresponding particle size distributions by measuring more than 200 particles from different regions. In the catalyst samples supported on GO and NiAl-LDH/RGO (Figure 7a and c), the average size of Au particles were 2.92 nm and 2.63 nm, respectively, which were much smaller than that supported on NiAl-LDH (4.18 nm). Smaller particle size of Au NPs on GO was attributed to the oxygenic functional groups on the surface of support, which provided anchoring centers for Au NPs. As for Au/NiAl-LDH/RGO, although there was a decrease in the oxygenic functional groups on the surface of RGO, the added defect sites in NiAl-LDH/RGO composite could also impact the particle size distribution of the loading Au NPs and the large specific surface area was also a key factor. Moreover, the Au NPs supported on pure GO tended to aggregate in a small region, which will also cause an adverse impact on the catalytic activity.

Fig. 8 displays the Au 4f XPS spectra of Au/silicon wafers, Au/GO, Au/NiAl-LDH and Au/NiAl-LDH/RGO. The peaks with binding energies at 83.0-84.0 eV and 86.8-87.8 eV can be assigned to the electron transitions of Au 4f$_{7/2}$ and Au 4f$_{5/2}$, respectively.[50] Compared with the Au NPs supported on chemical inert carrier (silicon wafers), the Au 4f$_{7/2}$ peak of Au NPs in Au/NiAl-LDH and Au/NiAl-LDH/RGO samples were shifted to lower binding energies by about 0.6 eV and 0.3 eV respectively, indicating that there was a stronger interaction between the Au particles and the NiAl-LDH or NiAl-LDH/RGO support. However, no such shift was observed for the Au/GO catalyst. In consequence, the introduction of the NiAl-LDH could strengthen the metal-support interaction and enhance the alcohol oxidation activity of catalyst.
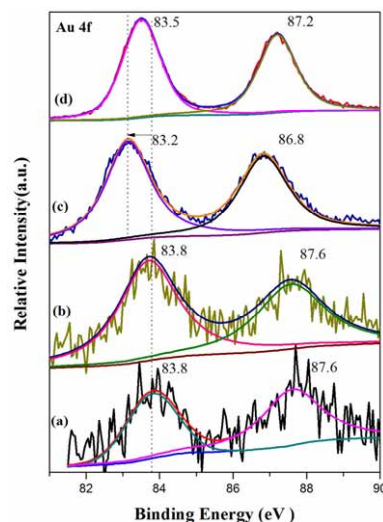

Fig. 8 Au 4f XPS of Au/silicon wafers (a), Au/GO (b), Au/NiAl-LDH (c) and Au/NiAl-LDH/RGO (d).

The catalytic oxidation of benzyl alcohol under solvent-free condition was investigated at 140 ^{o}C with 2 bar oxygen using a stainless steal autoclave and the results were shown in Fig. 9 and Table 1. The benzyl alcohol conversion of 1% Au/RGO is nearly same with 1% Au/GO catalysts and both in a relative low level. However, the benzaldehyde selectivity of Au/RGO catalysts was significantly higher than the catalysts supported with pure GO, which confirmed that superabundant oxygenic functional groups in GO facilitated the over-oxidation of benzyl alcohol and decrease the benzaldehyde selectivity. The benzyl alcohol conversion of 1%Au/NiAl-LDH/RGO catalyst reached ca. 62% after 10 h, higher than Au/GO, Au/RGO and Au/NiAl-LDH catalysts, which illustrated a very pronounced promotion of NiAl-LDH/RGO support to the oxidation of benzyl alcohol. The catalytic performance of the physical mixture of Au/GO and Au/NiAl-LDH catalysts as shown in Table.1 was between the two single support catalysts and much lower than Au/NiAl-LDH/RGO catalyst, which indicated that there was synergistic effect between RGO and NiAl-LDH in the composite support. The activity of Au/NiAl-LDH/RGO catalyst was 8.7 times higher than Au/GO catalyst, attributing to the introduction of NiAl-LDH with an abundance of basic sites and transition metal cations. 1.2 times higher than Au/NiAl-LDH catalyst can be ascribed to smaller Au particle size benefiting from the oxygenic functional groups and defect sites in RGO.
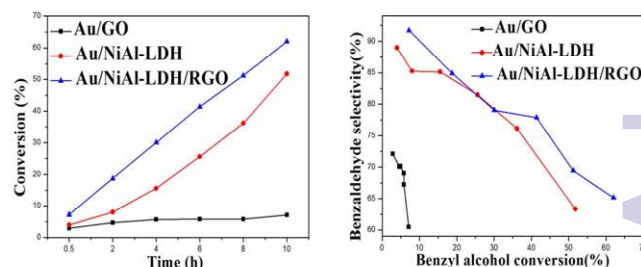

Fig. 9 Catalytic performance of 1% Au catalysts supported on GO, NiAl-LDH and NiAl-LDH/RGO.

Table 1. Catalytic performance of Au catalysts with different supports.

Catalysts	Specific surface area (m^2/g)	Au loading (wt. %)	Mean Au size (nm)	Conversion (%)	Selectivity (%)	TON[a]
Au/GO	136.93	0.52	2.92	7.1	60.6	2604.7
Au/RGO	141.89	0.65	2.89	6.3	82.1	2724.6
Au/NiAl-LDH	61.18	0.82	4.18	51.8	63.3	12024.9
Au/NiAl-LDH/RGO	172.47	0.66	2.63	62.0	65.2	17893.4
Au/GO + Au/NiAl-LDH[b]	—	0.75	—	38.2	60.2	9686.8

[a] TON values were calculated with respect to the total loading of Au after 10 h reaction.

[b] Au/GO + Au/NiAl-LDH is the physical mixture of Au/GO and Au/NiAl-LDH

Even the Au loadings of four catalysts are different, the trend of TON in Table.1 was in accordance with the activity, and the Au/NiAl-LDH/RGO catalyst had the highest TON. In addition, when comparing the selectivity towards benzaldehyde at iso-conversion of benzyl alcohol, the selectivity of Au/NiAl-LDH/RGO catalyst is nearly equal with Au/NiAl-LDH catalyst but considerably higher than Au/GO catalyst, which may be attributed to the surface properties of LDH and less oxygenic functional groups of RGO, preventing the over-oxidation of benzyl alcohol.

Besides the target product of benzaldehyde, there were still a number of by-products formed by oxidation of benzyl alcohol e.g. toluene, benzoic acid, benzyl benzoate. Fig. 10 shows the selectivity towards by-products as a function of benzyl alcohol conversion for the Au/GO, Au/NiAl-LDH and Au/NiAl-LDH/RGO catalysts. All three catalytic selectivity to toluene maintained in a relative low level (< 10%). In the case of Au/GO catalyst, the major by-product in benzyl alcohol oxidation was benzoic acid, and a few benzyl benzoate was also produced. However, the reaction catalyzed by Au/NiAl-LDH and Au/NiAl-LDH/RGO barely produced benzoic acid but the selectivity towards benzyl benzoate increased to ca. 35%. It is possible that benzaldehyde reacted with benzyl alcohol to form a hemiacetyl and it was oxidized to benzyl benzoate, which means there are two different reaction routes catalyzed by Au/GO and Au/NiAl-LDH catalyst.[51] Compared with Au/GO catalyst, the Au/NiAl-LDH exhibited preferable selectivity to the target product, and the Au/NiAl-LDH/RGO catalyst inherited this advantage.

The effect of the GO/NiAl-LDH ratio on activity and selectivity was investigated and the results were shown in Fig. 11. The GO/NiAl-LDH ratio was achieved by turning the mass ratio of GO and $Ni(NO_3)_2·6H_2O$ precursor. An increase in catalytic activity was observed with the content of NiAl-LDH increasing. This increase of activity reached a maximum with a GO/$Ni(NO_3)_2·6H_2O$ mass ratio of 1:2.8. A further increase in the NiAl-LDH content resulted in a decrease in the catalytic activity. It is important to note that in the presence of a minor amount of NiAl-LDH (1:1.4 GO/ $Ni(NO_3)_2·6H_2O$ mass ratio), there was no obvious increase in the catalytic activity, but the benzaldehyde

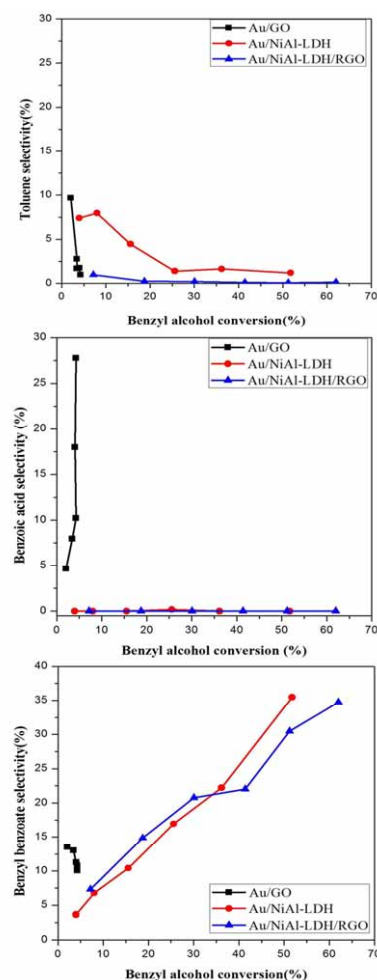selectivity was significantly higher than the catalysts supported with pure GO.


Fig. 10 Selectivity to toluene, benzoic acid and benzyl benzoate as a function of benzyl alcohol conversion over 1% Au catalysts supported by GO, NiAl-LDH and NiAl-LDH/RGO.

This phenomenon is similar with the fact that the selectivity of Au/RGO is better than Au/GO, mainly attributed to the reduction of GO in accompany with the growth of NiAl-LDH. In summary, the optimum selective oxidation of benzyl alcohol to benzaldehyde occured for the GO/ $Ni(NO_3)_2 \cdot 6H_2O$ 1:2.8 mass ratio support with the yield of 40%.
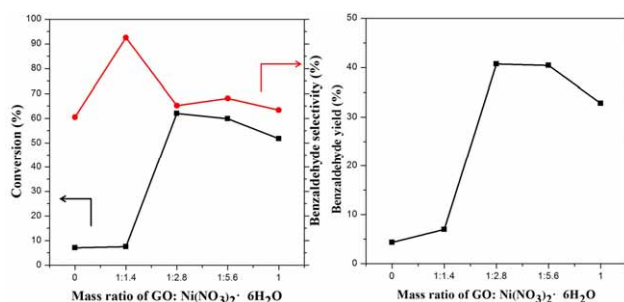

Fig. 11 The effect of GO/NiAl-LDH ratio on the benzyl alcohol conversion, selectivity to benzaldehyde and yield (reaction time: 10 h).

The reusability of the catalyst is also one of the key factors. After reaction, the catalysts were separated from the reaction mixture by centrifugation, thoroughly washed with acetone and then reused in the next reaction under the same conditions. The reusability of the catalysts supported on GO, NiAl-LDH and NiAl-LDH/RGO were investigated for three successive reactions and the results were shown in Fig. 12. After third recycling, the conversion of Au/GO and Au/NiAl-LDH catalysts dropped by 49.8% and 18.3%, respectively, while for Au/NiAl-LDH/RGO catalyst, the conversion only dropped by 10.0% and the selectivity of benzaldehyde still reached ca. 68%. HRTEM images of the used Au catalysts are shown in Fig. 13. For Au/NiAl-LDH catalyst, the average size of Au NPs after three times used was up to 8.93 nm, and the obvious agglomeration of Au NPs was observed. Therefore, the decrease in catalytic activity for Au/NiAl-LDH catalyst was mainly due to the agglomeration of Au NPs. A obvious deactivation was also observed in the catalyst supported on pure GO, however, the Au NPs were still uniformly scattered on the surface of both GO and NiAl-LDH/RGO support without obvious agglomeration, and the average size of Au NPs in the used Au/GO and Au/ NiAl-LDH/RGO catalyst were 5.15 nm and 4.93 nm. As the particle sizes of Au NPs supported on GO and NiAl-LDH/RGO were similar, the main reason for the deactivation could possibly be the agglomeration of GO, which partly covered the active sites. In contrast, the Au/NiAl-LDH/RGO catalyst was found to be fully reusable which attributed to the defect sites and oxygenic functional groups in RGO could anchor the Au NPs and prevent the agglomeration, meanwhile, the agglomeration of RGO was inhibited by the growth of NiAl-LDH. Therefore, the Au/NiAl-LDH/RGO catalyst possessed not only higher activity and benzaldehyde selectivity but also good stability during the solvent-free oxidation of benzyl alcohol.
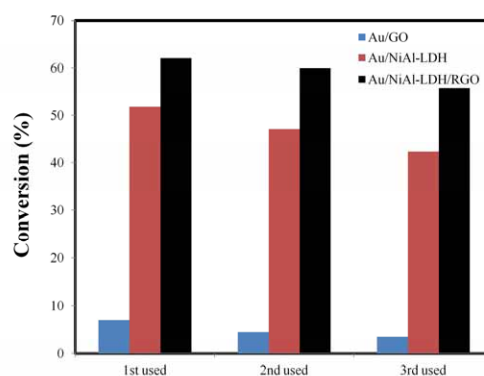
Fig. 12 Reusability of 1% Au catalysts supported by GO, NiAl-LDH and NiAl-LDH/RGO.
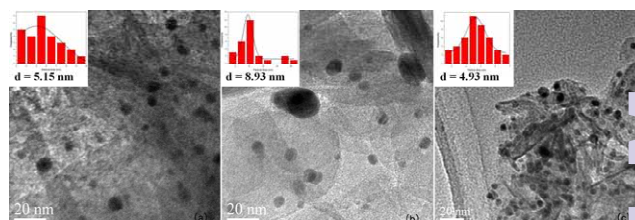
Fig. 13 HRTEM images and the size distribution of the used Au/GO (a), Au/NiAl-LDH (b) and Au/NiAl-LDH/RGO (c).

Conclusions

In the present work, a novel Au nanocatalyst supported on NiAl-LDH/RGO nanocomposite has been presented. The composite support was prepared via a coprecipitation process of NiAl-LDH on the surface of GO accompanied by the reduction of GO to RGO in alkaline solution. The formation of NiAl-LDH/RGO composite was confirmed by XRD and FT-IR. TEM observation of NiAl-LDH/RGO confirmed that the graphene sheets were decorated densely by nanosized NiAl-LDH particles and no obvious aggregate was observed. Raman spectroscopy and XPS analysis revealed that there were both defect sites and oxygenic functional groups in NiAl-LDH/RGO composite, which could be utilized as anchoring centers for the nucleation and dispersion of the Au nanoparticles and led to a smaller particle size. The average size of Au nanoparticles supported on GO, NiAl-LDH and NiAl-LDH/RGO were 2.92 nm, 4.18 nm and 2.63 nm, respectively. The synthesized Au/NiAl-LDH/RGO catalyst showed preferable catalytic performance including activity, selectivity and stability in the selective oxidation of benzyl alcohol. Improved activity was mainly ascribed to the small size of Au nanoparticles which controlled by RGO. Preferable selectivity to benzaldehyde was owing to the surface properties of NiAl-LDH as well as appropriate oxygenic functional groups in RGO which prevented the over-oxidation of benzyl alcohol. Moreover, superior catalytic stability of Au/NiAl-LDH/RGO catalyst was attributed to the defect sites and oxygenic functional groups in RGO which anchored the Au NPs and prevented the agglomeration, meanwhile, the agglomeration of RGO was inhibited by the introduction of NiAl-LDH. Thus, it can be seen that NiAl-LDH/RGO composite maintained the advantages of both RGO and NiAl-LDH, which enable it as a promising catalyst support in the selective oxidation of benzyl alcohol.

Acknowledgements

Notes and references

* *State Key Laboratory of Chemical Resource Engineering, Beijing University of Chemical Technology, 100029, Box 98, 15 Bei San Huan East Road, Beijing, 10002 , China*
Fax: +86 (10) 6442 5385; Tel: +86 (10) 6445 1007;
E-mail address:
lidq@mail.buct.edu.cn *(D. Q. Li)*
fengjt@mail.buct.edu.cn *(J. T. Feng)*

1 Z. Guo, B. Liu, Q. H. Zhang, W. P. Deng, Y. Wang and Y. H. Yang, *Chem. Soc. Rev.*, 2014, **43**, 3480-3524.

2 N. Dimitratos, J. A. Lopez-Sanchez, D. Morgan, A. F. Carley, R. Tiruvalam, C. J. Kiely, D. Bethella and G. J. Hutchings, *Phys. Chem. Chem. Phys.*, 2009, **11**, 5142-5153.

3 W. Feng, G. J. Wu, L. D. Li and N. J. Guan, *Green Chem.*, 2011, **13**, 3265-3272.

4 A. Thomas, Q. He and J. K. Edwards, *Faraday Discuss.*, 2011, **152**, 381-392.

5 Y. L. Hong, X. L. Jing, J. L. Huang, D. H. Sun, T. Odoom-Wubah, F. Yang, M. M. Du, and Q. B. Li, *ACS Sustainable Chem. Eng.*, 2014, **2**, 1752-1759.

6 V. R. Choudhary, R. Jha and P. Jana, *Green Chem.*, 2007, **9**, 267-272.

7 N. Dimitratos, J. A. Lopez-Sanchez and G. J. Hutchings, *Chem. Sci.*, 2012, **3**, 20-44.

8 G. L. Hallett-Tapley, M. J. Silvero, C. J. Bueno-Alejo, M. González-Béjar, C. D. McTiernan, M. Grenier, J. C. Netto-Ferreira and J. C. Scaiano, *J. Phys. Chem. C*, 2013, **117**, 12279-12288.

9 L. C. Wang, Y. M. Liu, M. Chen, Y. Cao, H. Y. He and K. N. Fan, *J. Phys. Chem. C*, 2008, **112**, 6981-6987.

10 T. A. G. Silva, R. Landersb and L. M. Rossi, *Catal. Sci. Technol.*, 2013, **3**, 2993-2999.

11 A. Villa, C. E. Chan-Thaw, G. M. Veith, K. L. More, D. Ferri and L. Prati, *ChemCatChem*, 2011, **3**, 1612-1618.

12 S. E. Davis, M. S. Ide and R. J. Davis, *Green Chem.*, 2013, **15**, 17-45.

13 F. Z. Zhang, X. F. Zhao, C. H. Feng, B. Li, T. Chen, W. Lu, X. D. Lei and S. L. Xu, *ACS Catal.*, 2011, **1**, 232-237.

14 A. Mondal and N. R. Jana, *ACS Catal.*, 2014, **4**, 593-599.

15 M. I. Katsnelson, *Materials today*, 2007, **10**, 20-27.

16 L. Liao, H. L. Peng and Z. F. Liu, *J. Am. Chem. Soc.*, 2014, **136**, 12194-12200.

17 M. Sun, H. J. Liu, Y. Liu, J. H. Qu and J. H. Li, *Nanoscale*, 2013, **00**, 1-3.

18 N. N. Zhang, H. X. Qiu, Y. Liu, W. Wang, Y. Li, X. D. Wang and J. P. Gao, *J. Mater. Chem.*, 2011, **21**, 11080-11083.

19 B Garg, Y. C. Ling, *Green Materials*, 2013, **1**, 47-61.

20 D. R. Dreyer, H. P. Jia and C. W. Bielawski, *Angew. Chem. Int. Ed.*, 2010, **49**, 6813-6816.

21 E. Yoo, T. Okata, T. Akita, M. Kohyama, J. Nakamura, and I. Honma, *Nano Lett.*, 2009, **9**, 2255-2255.

22 G. M. Scheuermann, L. Rumi, P. Steurer, W. Bannwarth and R. Mülhaupt, *J. Am. Chem. Soc.*, 2009, **131**, 8262-8270.

23 P. Sharma, G. Darabdhara, T. M. Reddy, A. Borah, P. Bezboruah, P. Gogoi, N. Hussain, P. Sengupta, M. R. Das, *Catalysis Communications*, 2013, **40**, 139-144.

24 B. J. Hong, O. C. Compton, Z. An, I. Eryazici and S. T. Nguyen, *ACS nano*, 2011, **6**, 63-73.

25 P. Sharma, G. Darabdhara, T. M. Reddy, A. Borah, P. Bezboruah, P. Gogoi, N. Hussain, P. Sengupta and M. R. Das, *Catalysis Communications*, 2013, **40**, 139-144.

26 K. M. Parida, L. Mohapatra, *Chem. Eng. J*, 2012, **179**, 131-139.

27 G. L. Fan, F. Li, D. G. Evans and X. Duan, *Chemical Society Reviews*, 2014, **43**, 7040-7066.

28 M. F. Shao, F. Y. Ning, J. W. Zhao, M. Wei, D. G. Evans and X. Duan, *Adv. Funct. Mater.*, 2013, **23**, 3513-3518.

29 B. Ballarin, A. Mignani, E. Scavetta, M. Giorgetti, D. Tonelli, E. Boanini, C. Mousty and V. Prevot, *Langmuir*, 2012, **28**, 15065-15074.

30 K. M. Parida, M. Sahoo, S. Singha, *J. Catal.*, 2010, **276**, 161-169.

31 Z. Gao, J. Wang, Z. S. Li, W. L. Yang, B. Wang, M. J. Hou, Y. He, Q. Liu, T. Mann, P. P. Yang, M. L. Zhang and L. H. Liu, *Chem. Mater.*, 2011, **23**, 3509-3516.

32 M. Lan, G. L. Fan, L. Yang and F. Li, *Ind. Eng. Chem. Res.*, 2014, **53**, 12943-12952.

33 X. B. Fan, W. C. Peng, Y. Li, X. Y. Li, S. L. Wang, G. L. Zhang and F. B. Zhang, *Adv. Mater.*, 2008, **20**, 4490-4493.

34 R. F. Xie, G. L. Fan, Q. Ma, L. Yang and F. Li, *J. Mater. Chem. A*, 2012, **00**, 1-3.

35 L. L. Geng, S. J. Wua, Y. C. Zou, M. J. Jia, W. X. Zhang, W. F. Yan, G. Liu, *Journal of Colloid and Interface Science*, 2014, **42**, 71-77.

36 H. Wang, X. Xiang and F. Li, *J. Mater. Chem.*, 2010, **20**, 3944-3952.

37 L. Li, R. Z. Ma, Y. Ebina, K. Fukuda, K. Takada and T. Sasaki, *J. Am. Chem. Soc.*, 2007, **129**, 8000-8007.

38 J. Xu, S. Gai, F. He, N. Niu, P. Gao, Y. J. Chen and P. P. Yang, *J. Mater. Chem. A*, 2014, **2**, 1022-1031.

39 C. L. Bao, L. Song, W. Y. Xing, B. H. Yuan, C. A. Wilkie, J. L. Huang, Y. Q. Guo and Y. Hu, *J. Mater. Chem.*, 2012, **22**, 6088-6096.

40 S. L. Ma, C. H. Fan, L. Du, G. L. Huang, X. J. Yang, W. P. Tang, Y. Makita and K. Ooi, *Chem. Mater.*, 2009, **21**, 3602-3610.

41 Y. J. Feng, Y. Jiang, Q. Huang, S. T. Chen, F.B Zhang, P. G. Tang and D. Q. Li, *Ind. Eng. Chem. Res.*, 2014, **53**, 2287-2292.

42 X. Q. Xie, J. L. Long, J. Xu, L. M. Chen, Y. Wang, Z. Z. Zhang and X. X. Wang, *RSC Advances*, 2012, **2**, 12438-12446.

43 F. F. Ren, C. Q. Wang, C. Y. Zhai, F. X. Jiang, R. R. Yue, Y. K. Du, P. Yang and J. K. Xu, *J. Mater. Chem. A*, 2013, **1**, 7255-7261.

44 E. G. Rodrigues, J. J. Delgado, X. Chen, M. F. R. Pereira and J. J. M. Órfão, *Ind. Eng. Chem. Res.*, 2012, **51**, 15884-15894.

45 M. X. Li, J. E. Zhu, L. L. Zhang, X. Chen, H. M. Zhang, F. Z. Zhang, S. L. Xu and D. G. Evans, *Nanoscale*, 2011, **3**, 4240-4246.

46 X. Wang, S. Zhou, W. Y. Xing, B. Yu, X. M. Feng, L. Song and Y. Hu, *J. Mater. Chem. A*, 2013, **1**, 4383-4390.

47 W. H. Fang, J. S. Chen, Q. H. Zhang, W. P. Deng and Y. Wang, *Chem. Eur. J.*, 2011, **17**, 1247-1256.

48 J. Wang, X. J. Lang, B. Zhaorigetu, M. L. Jia, J. Wang, X. F. Guo and J. C. Zhao, *ChemCatChem*, 2014, **6**, 1737-1747.

49 J. T. Feng, C. Ma, P. J. Miedziak, J. K. Edwards, G. L. Brett, D. Q. Li, Y. Y. Du, D. J. Morganb and G. J. Hutchings, *Dalton Trans.*, 2013, **42**, 14498-14508.